Neuron, Vol. 45, 405–417, February 3, 2005, Copyright ©2005 by Elsevier Inc. DOI 10.1016/j.neuron.2004.12.048

# Presynaptic Action Potential Amplification by Voltage-Gated $Na^+$ Channels in Hippocampal Mossy Fiber Boutons

**Dominique Engel and Peter Jonas***
Physiologisches Institut der Universität Freiburg
Hermann-Herder-Strasse 7
D-79104 Freiburg
Germany

## Summary

**Action potentials in central neurons are initiated near the axon initial segment, propagate into the axon, and finally invade the presynaptic terminals, where they trigger transmitter release. Voltage-gated $Na^+$ channels are key determinants of excitability, but $Na^+$ channel density and properties in axons and presynaptic terminals of cortical neurons have not been examined yet. In hippocampal mossy fiber boutons, which emerge from parent axons en passant, $Na^+$ channels are very abundant, with an estimated number of ~2000 channels per bouton. Presynaptic $Na^+$ channels show faster inactivation kinetics than somatic channels, suggesting differences between subcellular compartments of the same cell. Computational analysis of action potential propagation in axon-multibouton structures reveals that $Na^+$ channels in boutons preferentially amplify the presynaptic action potential and enhance $Ca^{2+}$ inflow, whereas $Na^+$ channels in axons control the reliability and speed of propagation. Thus, presynaptic and axonal $Na^+$ channels contribute differentially to mossy fiber synaptic transmission.**

## Introduction

Communication between excitable cells is a complex series of electrical and chemical events. Following initiation near the initial segment, action potentials (APs) propagate into the axon, invade the presynaptic terminals, and finally trigger transmitter release (Hille, 2001; Katz, 1969). Whereas the propagation of the AP along the axon is an active process critically dependent on a high density of voltage-gated $Na^+$ channels, the process of AP invasion into presynaptic terminals is less well understood. While there is evidence for active invasion in the amphibian neuromuscular junction (Katz and Miledi, 1965), APs are thought to spread passively from the preterminal heminode into the terminal branches in mouse and lizard neuromuscular synapses (Brigant and Mallart, 1982; Dreyer and Penner, 1987; Lindgren and Moore, 1989). Furthermore, direct presynaptic recordings from the rat calyx of Held, a major relay synapse in the auditory brainstem, revealed that $Na^+$ channels are clustered near the heminode, but are excluded from the presynaptic calyceal terminal (R.M. Leão et al., 2004, Soc. Neurosci., abstract). Thus, at least in mammalian neuromuscular junctions and calyx synapses, AP invasion into presynaptic terminals appears to be a passive process.

*Correspondence: peter.jonas@physiologie.uni-freiburg.de

Is the absence of $Na^+$ channels from presynaptic terminals a general phenomenon that also extends to cortical boutons? Unlike peripheral axons, central axons often show extensive branching, and the majority of synaptic boutons emerge from these axons in an en passant manner. Both axonal branches and en passant boutons may generate a substantial electrical load to the invading AP (Goldstein and Rall, 1974; Lüscher and Shiner, 1990a, 1990b). Although the reliability of conduction of APs in cortical axons remains controversial (Koester and Sakmann, 2000; Cox et al., 2000; Debanne et al., 1997; reviewed by Debanne, 2004), computational studies have suggested that AP propagation may fail at axonal branch points and en passant boutons, leading to presynaptically silent synapses (Lüscher and Shiner, 1990a, 1990b). Furthermore, strings of large en passant boutons may generate substantial delays in propagation (Manor et al., 1991). The role of $Na^+$ channels in the process of AP propagation and coupling to transmitter release has remained unclear. While the presence of $Na^+$ channels in presynaptic elements may be necessary to ensure fast and reliable AP propagation, the absence of $Na^+$ conductances could be beneficial for limiting AP duration, as required for the precise timing of transmitter release (R.M. Leão et al., 2004, Soc. for Neurosci. abstract; Geiger and Jonas, 2000; Sabatini and Regehr, 1999).

The hippocampal mossy fiber pathway, the major connection from the dentate gyrus to the CA3 region, appears to be an ideal system in which these questions can be directly addressed (Henze et al., 2002; Bischofberger and Jonas, 2002). The mossy fiber is a thin, unmyelinated axon, from which several large en passant boutons (MFBs; 3–5 μm in diameter; average number, 14) emerge (Amaral et al., 1990; Chicurel and Harris, 1992). Additionally, filopodial extensions originate from the large boutons (Acsády et al., 1998). The goals of this study were (1) to test by direct recording whether mossy fiber boutons have active properties, (2) to examine whether the gating of presynaptic $Na^+$ channels differs from that of somatic channels, and (3) to study with computational approaches AP propagation in mossy fiber axons, boutons, and filopodial extensions. We find that mossy fiber boutons, in contrast to previously examined presynaptic terminals, have active properties, expressing $Na^+$ channels in high density. Surprisingly, boutons act as sites of boosting of the AP amplitude rather than failure of AP propagation.

## Results

### Hippocampal Mossy Fiber Boutons Have Active, Axon-like Properties

To address whether presynaptic elements in cortical circuits have active properties, we attempted to record $Na^+$ currents in outside-out patches isolated from hippocampal MFBs (Figure 1). After block of voltage-gated $K^+$ channels and $Ca^{2+}$ channels by a combination of external TEA + 4-AP + $Cd^{2+}$ and internal $Cs^+$, test pulses

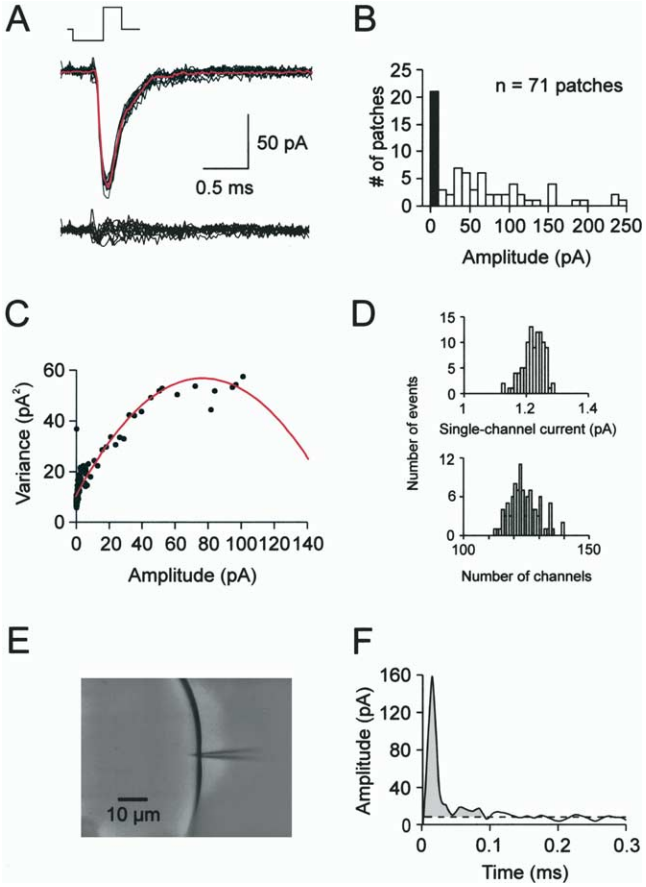


Figure 1. High $Na^+$ Channel Density in Hippocampal Mossy Fiber Boutons

(A) Upper panel, ensemble of 10 consecutive traces of $Na^+$ currents recorded from an outside-out patch isolated from an MFB, superimposed with the mean current trace (red). Lower panel, deviations of individual traces from the mean. Pulse protocol: holding potential, –80 mV, 50 ms prepulse to –120 mV, and 30 ms test pulse to 0 mV.

(B) Histogram of $Na^+$ peak current in presynaptic patches (test pulse, 0 mV). Filled bar indicates a subset of patches entirely lacking voltage-dependent currents (presumably vesicles). Data from 71 patches.

(C) Plot of ensemble variance against ensemble mean for a total of 100 traces. Continuous curve is a parabolic function fitted to the data points. Same patch as in (A).

(D) Histograms of estimated single-channel current (top) and number of channels in the patch (bottom), obtained by bootstrap analysis for the experiment shown in (C) (see Experimental Procedures).

(E) Estimation of patch area based on direct measurement of the capacitance of outside-out patches. Light micrograph shows the experimental situation after insertion of patch pipette tip into a Sylgard ball.

(F) Difference of capacitive currents before and after insertion of the recording pipette tip into a Sylgard ball. Holding potential, –50 mV, test pulse to –100 mV. Dashed line indicates leakage current; gray area represents the integral under the capacitive component.

to 0 mV preceded by prepulses to –120 mV evoked large transient inward currents in 50 of 71 patches isolated from MFBs (Figure 1A). The peak amplitudes of the currents in individual patches ranged from 15.7–241.8 pA, with a mean ± standard error of the mean of 85.9 ± 8.4 pA (Figure 1B).

To determine the total number of $Na^+$ channels in a patch, we analyzed the macroscopic $Na^+$ currents by nonstationary fluctuation analysis (Sigworth, 1980). The ensemble variance was calculated from the fluctuation of $Na^+$ currents around the mean (Figure 1A), plotted against the ensemble mean, and fitted with a parabolic function (Figure 1C). In five MFB patches, the mean single-channel current $i$ was 0.91 ± 0.09 pA, and the estimated mean total channel number $N$ was 173 ± 19. Analysis of confidence intervals by bootstrap analysis confirmed that reliable parameter estimates could be obtained in all experiments (Figure 1D). Nonstationary fluctuation analysis also allowed us to determine the maximum open probability as $I_{peak}/(i\,N)$ = 0.529 ± 0.053 (n = 5).

To obtain quantitative estimates of conductance density and channel density, we further determined the membrane area of outside-out patches from their capacitance (Figures 1E and 1F; Sakmann and Neher, 1995). The capacitance of outside-out patches isolated from MFBs was 43.8 ± 4.5 fF (n = 7), corresponding to a patch area of 4.38 $\mu m^2$, assuming a specific membrane capacitance of 1 $\mu F\ cm^{-2}$. Using the mean values of macroscopic peak current, single-channel current, and measured patch area, we estimate a $Na^+$ conductance density of 49.0 $mS\ cm^{-2}$ (range: 9–138 $mS\ cm^{-2}$) and a presynaptic $Na^+$ channel density of 41 channels $\mu m^{-2}$ in hippocampal MFBs. These density values are comparable to previous estimates in invertebrate axons (120 $mS\ cm^{-2}$ in squid axons and 40 $mS\ cm^{-2}$ in Myxicola axons; Hodgkin and Huxley, 1952; Goldman and Schauf, 1973). Thus, presynaptic mossy fiber terminals have axon-like properties, expressing voltage-gated $Na^+$ channels in very high density.

### The Gating of Presynaptic $Na^+$ Channels

Understanding the role of presynaptic $Na^+$ channels in AP conduction in mossy fibers requires a quantitative analysis of $Na^+$ channel gating (Hodgkin and Huxley, 1952; Bezanilla and Armstrong, 1977; Taddese and Bean, 2002). We therefore analyzed the kinetics and voltage-dependence of gating (Figures 2 and 3). $Na^+$ currents in patches isolated from MFBs evoked by test pulses to 0 mV were transient, with a fast sigmoidal activation phase followed by a fast inactivation phase (Figures 1, 2A, and 2C). Inactivation of $Na^+$ channels in MFBs was virtually complete; the steady-state current measured 30 ms after the onset of the test pulse was only 0.90 ± 0.30% of the peak current (n = 9). Thus,

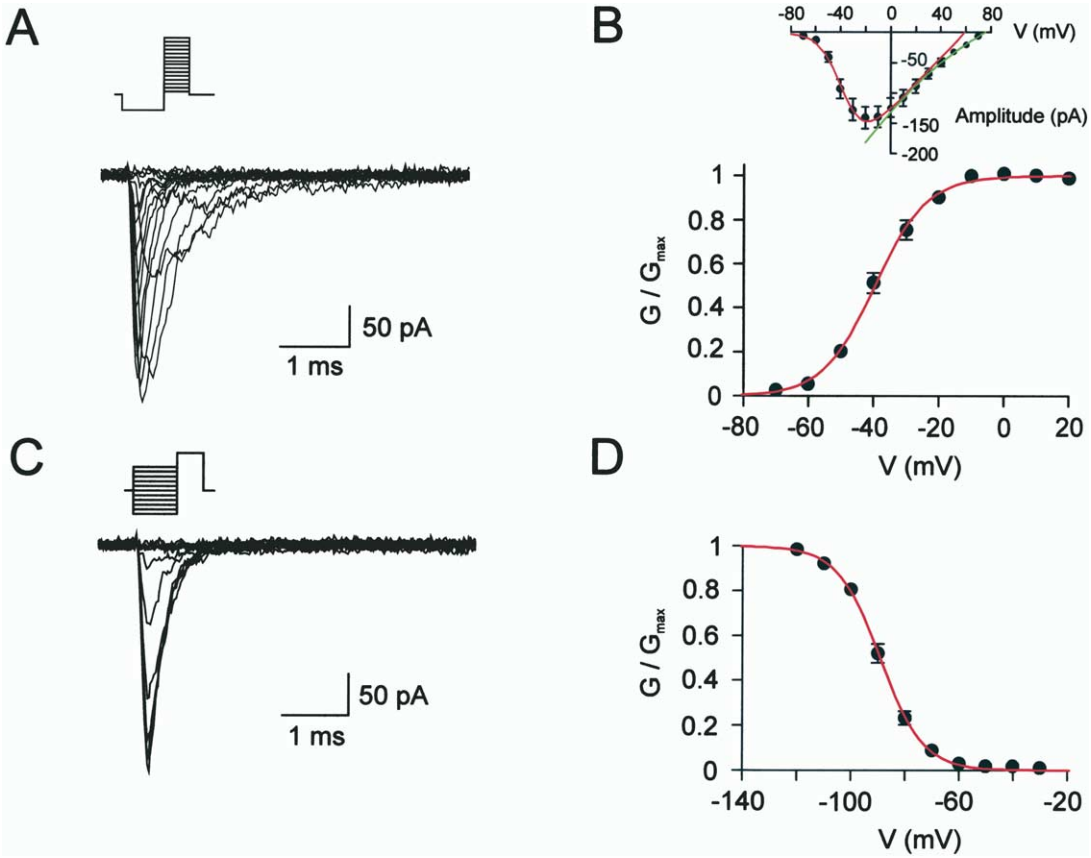


Figure 2. Voltage Dependence of Activation and Inactivation of $Na^+$ Channels in MFBs

(A) Traces of $Na^+$ current recorded from an outside-out patch isolated from an MFB at various test pulse potentials. Pulse protocol: holding potential, –80 mV, 50 ms prepulse to –120 mV, and 30 ms test pulse to potentials between –70 and +70 mV (10 mV increments).

(B) Activation curve. Conductance G was calculated from the $Na^+$ peak current and the reversal potential (see inset in [A]), normalized to the maximal value, and plotted against the test pulse potential (13 patches). Data were fitted with a Boltzmann function (continuous curve). The inset shows the mean peak $Na^+$ current-voltage (I-V) relation. Inverted bell-shaped curve (red) is the product of a Boltzmann function and a linear relation fitted to the data points. Convex curve (green) represents a 2nd order polynomial function fitted to the data points for voltages $\geq$10 mV.

(C) Steady-state inactivation induced by prepulses to different potentials. Pulse protocol: holding potential, –80 mV, 50 ms prepulse to voltages between –120 and –30 mV (10 mV increments), and 30 ms test pulse to 0 mV.

(D) Steady-state inactivation ($h_\infty$) curve. $Na^+$ peak current amplitude, normalized to the maximal $Na^+$ current, was plotted against the prepulse potential (13 patches). Data were fitted with a Boltzmann function (continuous curve).

the presynaptic $Na^+$ channels in MFBs were rapidly and completely inactivating.

The high channel density and the ideal voltage-clamp conditions in the isolated patch allowed us to measure the voltage-dependence and kinetics of gating with high resolution. To determine the activation curve, a major determinant of the threshold of AP initiation under physiological conditions, we used a pulse paradigm with test pulses ranging from –70 mV to +70 mV preceded by 50 ms prepulses to –120 mV. Activation curves were obtained by converting peak currents into peak conductances, normalizing them by the maximal value reached at potentials $\geq$ 0 mV, and plotting them against test pulse potential (Figures 2A and 2B). To measure the inactivation curve, a major determinant of $Na^+$ channel availability at varying resting potentials, we used a pulse paradigm with test pulses to 0 mV, preceded by 50 ms prepulses ranging from –120 mV to –30 mV. Steady-state inactivation was quantified as the ratio of peak currents at a given prepulse potential divided by the maximal $Na^+$ current (Figures 2C and 2D). Both activation and inactivation curves showed a sigmoidal shape and were fitted adequately by Boltzmann functions (see Table 1). The mean midpoint potential of the activation curve was –38.4 mV, and the slope factor was 8.0 mV (n = 13), corresponding to the movement of 3.2 elementary charges through the entire membrane electric field.

We next analyzed the time course of activation and inactivation of the presynaptic $Na^+$ channels. The activation time constant was obtained by fitting the rise of $Na^+$ currents at test pulse potentials $\geq$–50 mV with an exponential function with delayed onset (Figure 3A). The inactivation time constant was measured by fitting the decay of the $Na^+$ currents with an exponential function. To determine the deactivation time constant, we

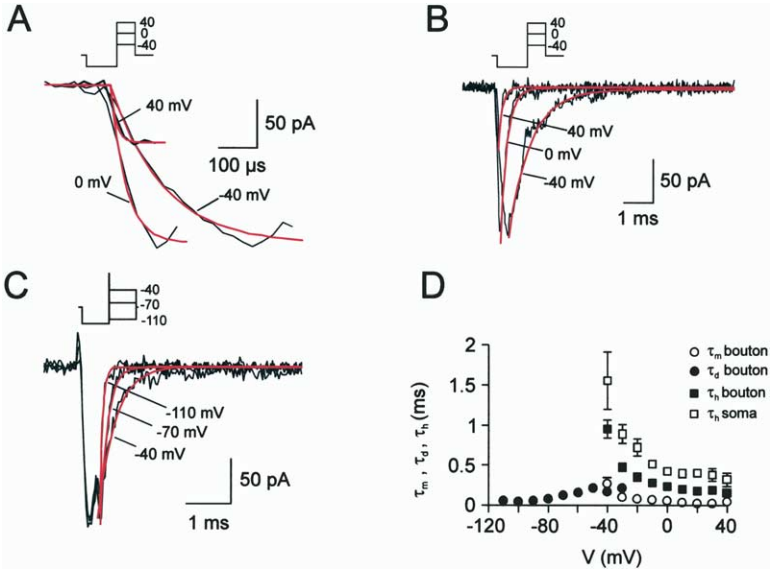


Figure 3. $Na^+$ Channels in MFBs Activate and Inactivate with Submillisecond Kinetics

(A) Time course of activation onset. The rising phase of the current was fitted with an exponential function with delayed onset. The corresponding fit curves are shown superimposed to the current traces. Time constants ($\tau_m$) = 132, 38, and 14 µs.

(B) Time course of inactivation onset. The decay phase of the current was fitted with an exponential function. Fit curves are shown superimposed. Pulse protocol for A and B: holding potential, –80 mV, 50 ms pulse to –120 mV, and test pulse to –40 mV, 0 mV, and 40 mV. Time constants ($\tau_h$) = 724, 221, and 146 µs. Same patch as in (A).

(C) Time course of deactivation. Pulse protocol: holding potential, –80 mV, 50 ms pulse to –120 mV, 300 µs pulse to 0 mV, and 50 ms test pulse to –110, –70, or –40 mV (see inset). The decay of the tail current at –110 and –70 mV was fitted monoexponentially, whereas the decay at –40 mV was fitted biexponentially. As the biexponential decay presumably arises from the temporal overlap of deactivation and inactivation (Oxford, 1981), the time constant of the fast component was taken as the deactivation time constant. The fit curves are shown superimposed. Time constants ($\tau_d$) = 69, 161, and 190 µs.

(D) Plot of activation $\tau_m$ (open circles), deactivation $\tau_d$ (filled circles), and inactivation $\tau_h$ (filled squares) against membrane potential. Deactivation time constants between –30 and –50 mV were obtained as the fast time constant of a biexponential fit. Inactivation time constants $\tau_h$ for somatic patches (open squares) are shown for comparison.

applied 300 µs pulses to 0 mV followed by steps to potentials between –110 and –30 mV (Figure 3C), and fitted the decay of the resulting $Na^+$ tail current with exponential functions. Activation and deactivation time constants plotted against voltage showed a bell-shaped relation, with a maximal value of 264 µs at –40 mV and minimal values of 45 µs at +40 mV (activation) and 51 µs at –110 mV (deactivation; Figure 3D; Table 1). Likewise, the inactivation time constant was 0.95 ms at –40 mV and decreased monotonically to 0.16 ms at +40 mV (Figures 4B and 4D; Table 1). Thus, presynaptic $Na^+$ channels inactivated very rapidly. A comparison of time constants of onset of inactivation in patches from MFBs and granule cell somata under identical recording conditions revealed that inactivation of presynaptic $Na^+$ channels was approximately two times faster than that of somatic $Na^+$ channels in the same cell type (Figure 3D; $P < 0.002$ for –30 mV).

The time course of inactivation in the subthreshold potential range is an important factor that determines $Na^+$ channel availability during repetitive activity. We therefore measured the time course of inactivation onset in prepulse experiments (Figures 4A and 4B) and the time course of recovery from inactivation with a double-pulse paradigm (Figures 4C and 4D). The time courses of both onset and recovery from inactivation were adequately fitted with a single exponential function. The time constant of onset of inactivation was 7.7 ms at –70 mV (n = 9; Figure 4B; Table 1), and the time constants of recovery from inactivation were 13.5 ms at

Table 1. Gating Properties of Presynaptic $Na^+$ Channels in MFBs

| | Activation | Deactivation | Inactivation | Recovery from Inactivation |
|---|---|---|---|---|
| Midpoint Potential | –38.4 ± 1.4 mV (n = 13; Figure 2B) | | –89.2 ± 1.2 mV (n = 13; Figure 2D) | |
| Slope Factor | 8.0 ± 0.5 mV (n = 13; Figure 2B) | | 6.4 ± 1.3 mV (n = 13; Figure 2D) | |
| τ | 264 ± 77 µs at –40 mV (n = 9; Figure 3A) | 170 ± 25 µs at –40 mV (n = 6; Figure 3C) | 0.95 ± 0.11 ms at –40 mV (n = 13; Figure 3B) | |
| τ | 45 ± 29 µs at +40 mV (n = 9; Figure 3A) | 51 ± 9 µs at –110 mV (n = 6; Figure 3C) | 0.16 ± 0.03 ms at +40 mV (n = 13; Figure 3B) | |
| τ (prepulse, double pulse) | | | 7.66 ms at –70 mV (n = 9; Figure 4B) | 4.70 ms at –120 mV (n = 10; Figure 4D) |
| | $\alpha_m$ | $\beta_m$ | $\alpha_h$ | $\beta_h$ |
| A | 93.8285 $ms^{-1}$ | 0.168396 $ms^{-1}$ | 0.000354 $ms^{-1}$ | 6.62694 $ms^{-1}$ |
| B | –105.023 mV | | | 17.6769 mV |
| C | 17.7094 mV | 23.2707 mV | 18.706 mV | 13.3097 mV |

$\alpha_m(V) = -A\ (V + B)/\{Exp[-(V+B)/C] - 1\}$
$\beta_m(V) = A\ Exp[-V/C]$
$\alpha_h(V) = A\ Exp[-V/C]$
$\beta_h(V) = A/\{Exp[-(V+B)/C] + 1\}$

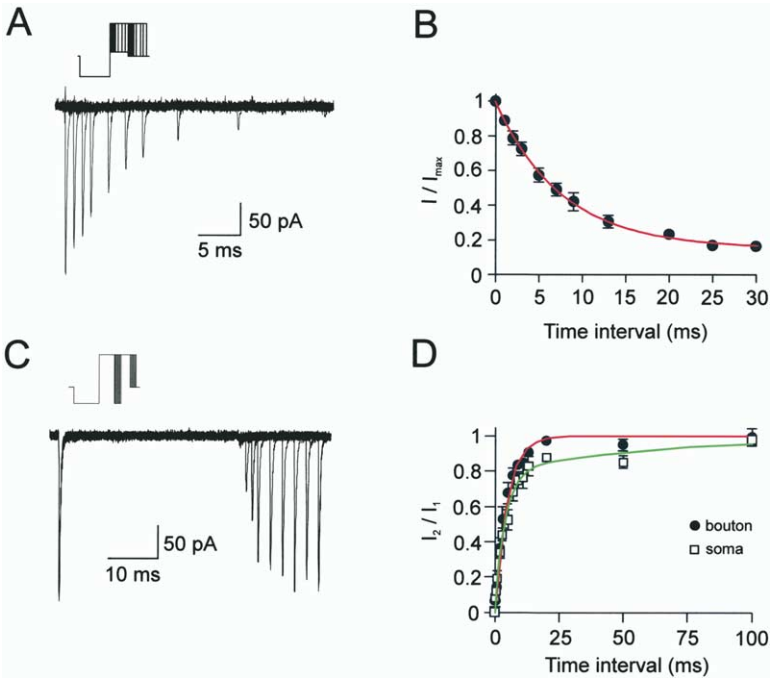


Figure 4. Na+ Channels in MFBs Show Fast Inactivation Onset and Recovery in the Subthreshold Voltage Range

(A) Time course of onset of inactivation from closed channel states. Pulse protocol: holding potential, −80 mV, 50 ms pulse to −120 mV, prepulse to −70 mV of variable duration, and 30 ms test pulse to 0 mV. First trace (left), Na+ current without prepulse.

(B) Na+ peak current amplitude, normalized to a response evoked by a test pulse without prepulse, was plotted against prepulse duration (9 patches). Curve represents exponential function fitted to the data points. The time constant was 7.66 ms.

(C) Time course of recovery from inactivation. Pulse protocol: holding potential, −80 mV, 50 ms pulse to −120 mV, 30 ms pulse to 0 mV (conditioning pulse), pulse of variable duration to −120 mV, 30 ms pulse to 0 mV (test pulse), and step back to −80 mV. Responses to the conditioning pulse (left); responses to the test pulse (right).

(D) Ratio of peak amplitude of the Na+ current evoked by the test pulse to that evoked by the conditioning pulse, plotted against the duration of the interpulse interval (10 patches). Filled circles, presynaptic patches; open squares, somatic patches. Data for presynaptic patches were fitted with a single exponential (red, time constant 4.70 ms). Data for somatic patches were fitted with the sum of two exponentials (green, time constants 4.05 ms [amplitude 0.8] and 64.5 ms [amplitude 0.2]; 7 patches).

−90 mV (n = 4) and 4.70 ms at −120 mV (n = 10; Figure 4D; Table 1). Recovery from inactivation was complete within ~10 ms at −120 mV. Thus, presynaptic Na+ channels recovered from inactivation very rapidly. In contrast, Na+ channels in granule cell somata under identical recording conditions showed a prominent slow component of recovery from inactivation (Figure 4D; $P < 0.05$ for 20 ms; Colbert et al., 1997; Jung et al., 1997; Martina and Jonas, 1997).

### Na+ Channels in MFBs Boost Presynaptic AP Amplitude and $Ca^{2+}$ Inflow

To examine the contribution of active boutons to AP propagation in mossy fibers, we described the gating of Na+ channels in MFBs by a Hodgkin-Huxley (HH)-type model. Figure 5 shows a summary of the total experimental data set, comprised of activation curve, activation and deactivation time constants, inactivation curve, inactivation time constant, and time constant of recovery from inactivation. The curves superimposed on the data show the prediction of the reparameterized HH model (see Table 1 for parameter values), illustrating that the model described the experimental observations adequately.

Next, we simulated AP conduction in a reduced but realistic axon-multibouton morphology comprised of a soma, 10 axonal segments of 100 µm length (surface area 63 $µm^2$), and 10 en passant boutons of 4 µm diameter (surface area 50 $µm^2$; Amaral et al., 1990; Figure 6). Na+ channels represented by the experimentally constrained HH model were inserted in different densities (the voltage dependence of both activation and inactivation was shifted by +12 mV to account for differences in the Donnan potential between whole-cell and isolated patch configuration; Fenwick et al., 1982; Marty and Neher, 1995). Figures 6A and 6B show plots of simulated voltage against time in the soma and all ten boutons, following the application of a depolarizing current stimulus at the soma.

We tested the hypothesis that MFBs are critical sites where AP propagation may fail (Lüscher and Shiner, 1990a, 1990b). Four scenarios were simulated: (1) a configuration in which both axon and boutons were endowed with a high Na+ conductance ($g_{Na,bouton} = g_{Na,axon} = 50$ mS $cm^{-2}$); (2) a similar scenario, but with passive boutons ($g_{Na,bouton} = 0$, $g_{Na,axon} = 50$ mS $cm^{-2}$); (3) a configuration in which axon and boutons were endowed with a reduced Na+ conductance ($g_{Na,bouton} = g_{Na,axon} = 15$ mS $cm^{-2}$); and (4) a similar scenario, but with passive boutons ($g_{Na,bouton} = 0$, $g_{Na,axon} = 15$ mS $cm^{-2}$). In the first scenario, the AP evoked by a single stimulus propagated reliably and with large amplitude (Figure 6A, left panel), consistent with reliable antidromic propagation of APs in mossy fiber axons observed experimentally (Schmitz et al., 2000; Ruiz et al., 2003). In the second situation, the reliability and conduction time were maintained, but the amplitude of the presynaptic AP was reduced substantially (Figure 6A, right panel). In the third scenario, the AP propagated reliably, but both AP amplitude and conduction velocity were reduced (Figure 6B, left panel). Finally, in the fourth scenario, AP propagation failed entirely (Figure 6B, right panel). Similar results were obtained with a 50 Hz train of 20 stimuli (Figures 6C and 6D).

Analysis of AP properties for a wide range of bouton and axon Na+ conductances revealed that the amplitude of the presynaptic AP and the probability of successful propagation were controlled differentially (Figures 6E and 6F). The presynaptic Na+ conductance

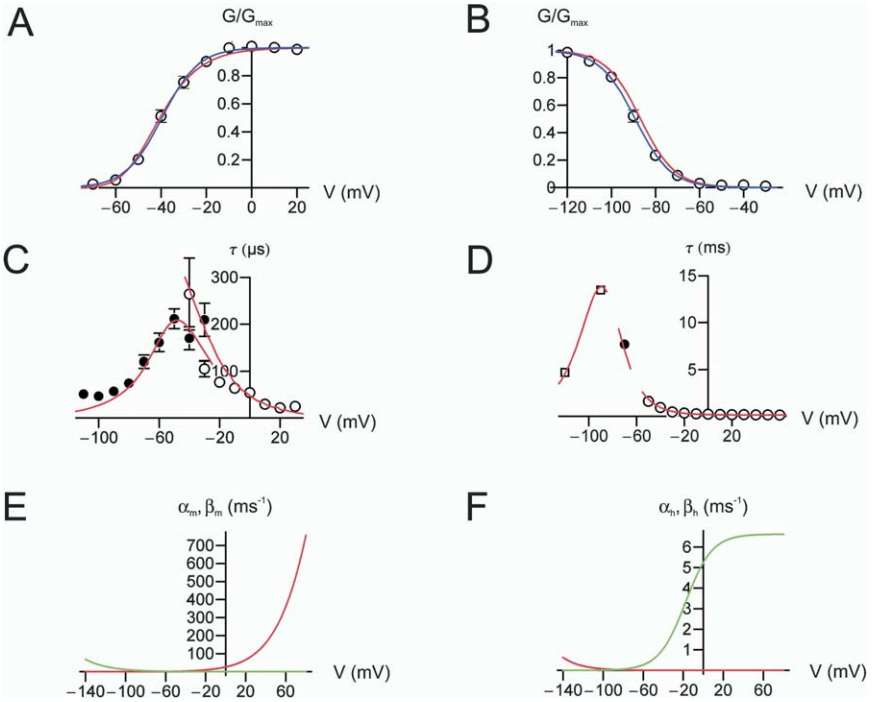


Figure 5. Modeling Presynaptic $Na^+$ Channel Gating with Hodgkin-Huxley Models of Activation and Inactivation

(A) Peak activation curve. (B) Steady-state inactivation ($h_\infty$) curve. Curves show prediction of HH model (red) and Boltzmann function fitted to the data points (blue). (C) Activation (open circles) and deactivation (filled circles) time constants. (D) Time constants of onset of inactivation from open state (open circles), inactivation from closed states measured by prepulse experiments (filled circles), and recovery from inactivation (open squares). Curves show prediction of the optimized HH model (red). (E and F) Voltage-dependence of $\alpha$ and $\beta$ of activation (E) and inactivation (F) of the optimized HH model. The best fit values of the rates are specified in Table 1.

density mainly determined the amplitude of the presynaptic AP, boosting it by 40 mV on average (Figures 6E and 6F). In contrast, the axonal $Na^+$ conductance density primarily influenced the reliability of propagation (Figures 6E and 6F). If the axon only, but not the boutons, had active properties, an axonal conductance of 20 mS $cm^{-2}$ was sufficient to ensure successful propagation. However, if only the boutons were active, a conductance of 80 mS $cm^{-2}$ was necessary. Thus, presynaptic and axonal $Na^+$ conductances have differential effects on AP propagation in mossy fiber axons. Presynaptic $Na^+$ channels boost the AP amplitude, whereas axonal $Na^+$ channels primarily determine the reliability of propagation.

We also tested the hypothesis that $Na^+$ channels in boutons are essential for the timing of signaling in the mossy fiber pathway, and we examined the conduction time and the half-duration of the presynaptic AP for a wide range of bouton and axon $Na^+$ conductances (Figures 7A and 7B). Increases in both bouton and axon $Na^+$ conductance density resulted in a decrease in conduction time. However, changes in conductance were less effective in the bouton than in the axonal compartment (Figure 7A). Likewise, increases in both bouton and axon $Na^+$ conductance density resulted in a decrease of the half-duration of the presynaptic AP, with $g_{Na,bouton}$ being slightly more effective than $g_{Na,axon}$ (Figure 7B). Thus, active properties of boutons contribute to the speed of AP propagation and, unexpectedly, to the short duration of the presynaptic AP.

The amplitude and shape of the presynaptic AP determines the amount of presynaptic $Ca^{2+}$ inflow, which in turn controls the amount of transmitter release (Geiger and Jonas, 2000; Bischofberger et al., 2002). This suggests that active boutons may contribute to boosting of synaptic strength at mossy fiber synapses. To test this possibility, we simulated presynaptic $Ca^{2+}$ currents evoked by the various presynaptic AP waveforms (Figure 7C), using a gating model of presynaptic high-voltage-activated $Ca^{2+}$ channels in MFBs (Bischofberger et al., 2002). For active boutons ($g_{Na,bouton}$ = $g_{Na,axon}$ = 50 mS $cm^{-2}$), the presynaptic peak $Ca^{2+}$ current was 2.8-fold larger than in a scenario with passive boutons ($g_{Na,bouton}$ = 0; $g_{Na,axon}$ = 50 mS $cm^{-2}$; Figure 7C). Analysis of AP amplitude for a wide range of bouton and axon $Na^+$ conductances revealed that presynaptic $Na^+$ channels typically boost presynaptic $Ca^{2+}$ inflow by a factor of ~2 (Figure 7C, inset).

Filopodial extensions, which emerge from the large bouton and form synapses on interneurons, are a hallmark of mossy fiber terminals (Acsády et al., 1998; Lawrence and McBain, 2003). The excitability of these filopodia is unknown. We simulated presynaptic $Ca^{2+}$ currents at the end of the filopodia in three different scenarios (Figure 7D): (1) a configuration in which both MFBs and filopodia were active ($g_{Na,bouton}$ = $g_{Na,filopodia}$ = 50 mS $cm^{-2}$), (2) a situation with active MFBs but passive filopodia ($g_{Na,bouton}$ = 50 mS $cm^{-2}$, $g_{Na,filopodia}$ = 0), and (3) a scenario in which both MFBs and filopodia were passive ($g_{Na,bouton}$ = $g_{Na,filopodia}$ = 0). The amplitude

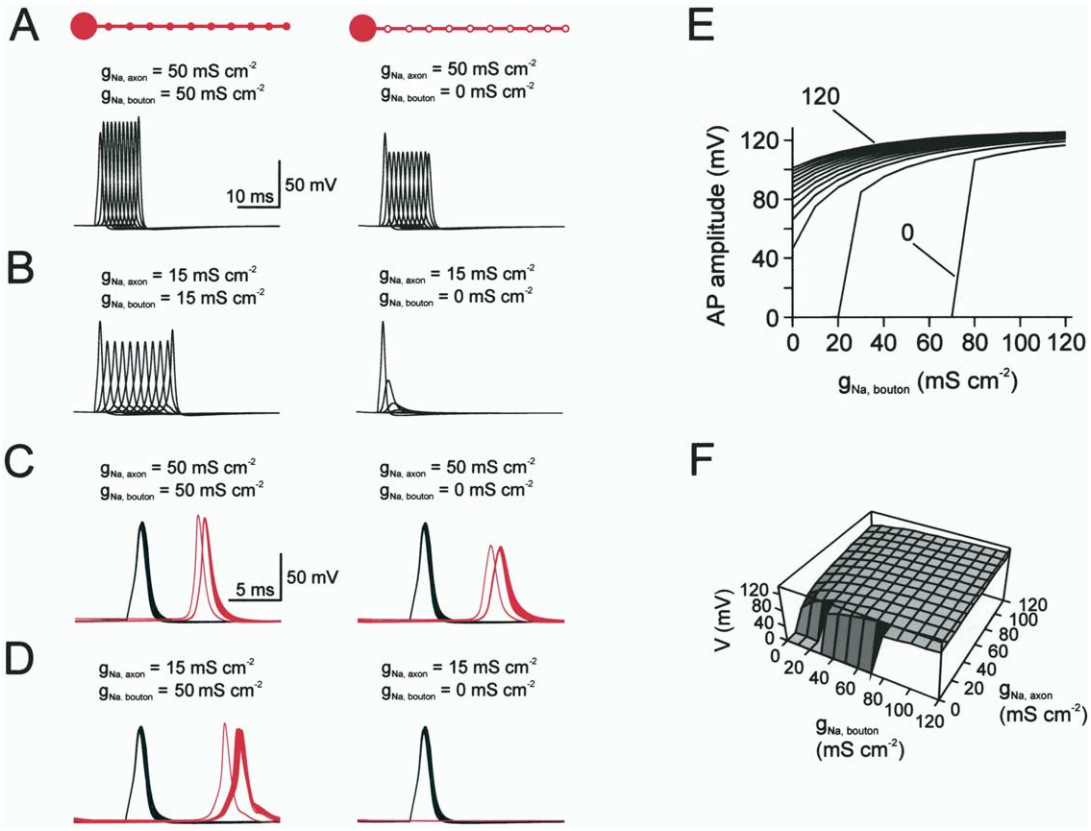


Figure 6. Na+ Channels in Boutons Amplify the Presynaptic AP Amplitude

(A and B) Simulation of orthodromic propagation of single APs in an axon-multibouton structure. Traces shown are APs in the soma (left) and the ten presynaptic terminals of the simulated structure. Conductance density $g_{Na,axon}$ = $g_{Na,bouton}$ = 50 mS cm$^{-2}$ ([A], left); $g_{Na,axon}$ = 50 mS cm$^{-2}$, $g_{Na,bouton}$ = 0 ([A], right); $g_{Na,axon}$ = $g_{Na,bouton}$ = 15 mS cm$^{-2}$ ([B], left); $g_{Na,axon}$ = 15 mS cm$^{-2}$, $g_{Na,bouton}$ = 0 ([B], right). Note that the AP is reliably propagated in all scenarios except the one with low $g_{Na,axon}$ and passive boutons, where propagation fails around the first bouton. Also note that the AP amplitude in the tenth bouton is slightly larger than in boutons 1–9, presumably due to reflection at the sealed end. (C and D) Simulation of propagation of a 50 Hz train of 20 APs in the same structure. Traces are APs in the soma (black) and the fifth bouton (red). Conductance density $g_{Na,axon}$ = $g_{Na,bouton}$ = 50 mS cm$^{-2}$ ([C], left); $g_{Na,axon}$ = 50 mS cm$^{-2}$, $g_{Na,bouton}$ = 0 ([C], right); $g_{Na,axon}$ = 15 mS cm$^{-2}$, $g_{Na,bouton}$ = 50 mS cm$^{-2}$ ([D], left); $g_{Na,axon}$ = 15 mS cm$^{-2}$, $g_{Na,bouton}$ = 0 ([D], right). Note the slight prolongation in conduction time from the 1st to the 20th AP in the train in C, left, which is further accentuated in the case of passive boutons ([C], right) and with reduced $g_{Na,axon}$. (E and F) Plot of AP amplitude at the fifth bouton (single somatic stimulus) measured from baseline against $g_{Na,bouton}$ for different values of $g_{Na,axon}$ (ranging from 0 to 120 mS cm$^{-2}$). The graph in (F) shows the same data plotted three-dimensionally against both $g_{Na,\ bouton}$ (front axis) and $g_{Na,axon}$ (right axis). Note that $g_{Na,bouton}$ determines the AP amplitude in the bouton (active boutons boost the AP by 40 mV in comparison to passive boutons), whereas $g_{Na,axon}$ has markedly smaller effects. APs were evoked by 200 pA, 2 ms current pulses at the soma. $g_{Na,soma}$ = 10 mS cm$^{-2}$ in all simulations.

of $I_{Ca}$ was large in the first, intermediate in the second, and very small in the third scenario (Figure 7D). Thus, active properties of boutons and/or filopodial extensions appear to be absolutely necessary to trigger glutamate release at mossy fiber-interneuron synapses (Lawrence and McBain, 2003).

## Discussion

Our results reveal several unexpected properties of hippocampal mossy fiber terminals. First, direct recording showed that mossy fiber boutons express Na+ channels in high density, in contrast to other presynaptic elements examined to date. Second, Na+ channels in MFBs show rapid inactivation onset and recovery, suggesting functional specialization of presynaptic versus somatodendritic channels. Finally, computational analysis revealed that presynaptic Na+ channels amplify the amplitude of the presynaptic AP, and thereby boost the presynaptic $Ca^{2+}$ inflow required for transmitter release. Thus presynaptic voltage-gated Na+ channels are involved in the control of synaptic transmission.

### Axon-like Properties of a Cortical Presynaptic Element

Based on recording of macroscopic Na+ currents in outside-out patches, we estimate a Na+ conductance density of 49 mS cm$^{-2}$ (or 490 pS μm$^{-2}$) and a Na+ channel density of 41 channels μm$^{-2}$ in hippocampal mossy fiber boutons (Figure 1). Assuming that the diameter of a typical bouton is 4 μm (Chicurel and Harris, 1992; Acsády et al., 1998; Geiger and Jonas, 2000), these values correspond to a total conductance of 24.6 nS and a total number of ~2000 channels per bouton. The pre-

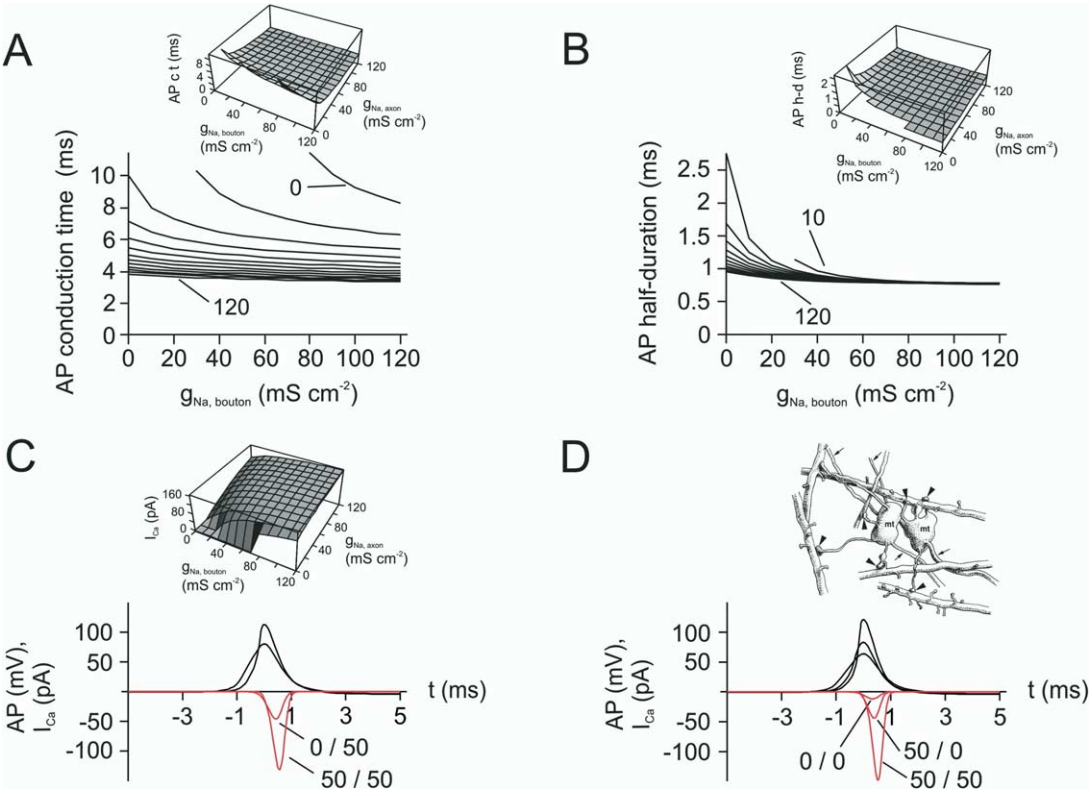


Figure 7. $Na^+$ Channels in Boutons Influence the Timing of Signaling and Boost Presynaptic $Ca^{2+}$ Inflow

(A) Plot of conduction time against $g_{Na,bouton}$ for various values of $g_{Na,axon}$ (0–120 mS cm$^{-2}$). Conduction time was measured as the time interval between the peaks of APs in the soma and the fifth bouton, which are spatially separated by 500 μm. (B) Plot of half-duration of AP in the fifth bouton against $g_{Na,bouton}$ for various values of $g_{Na,axon}$ (ranging from 0 to 120 mS cm$^{-2}$). (C) Simulation of presynaptic $Ca^{2+}$ inflow. APs at the fifth bouton (black) and corresponding $Ca^{2+}$ current (red) for active boutons (larger APs and currents) and passive boutons (smaller APs and currents). Note that active boutons increase the amplitude of the presynaptic $Ca^{2+}$ current by a factor ~2. Insets in (A)–(C) show a 3-D plot of conduction time, half-duration, and $Ca^{2+}$ peak current against both $g_{Na,bouton}$ (front axis) and $g_{Na,axon}$ (right axis). (D) AP shape and $Ca^{2+}$ inflow in filopodial extensions. Presynaptic APs and $Ca^{2+}$ current in the fifth large bouton and in a small terminal bouton of an attached filopodial extension (length, 30 μm). Active boutons and filopodia ($g_{Na,bouton}$ = $g_{Na,filopodium}$ = 50 mS cm$^{-2}$; largest trace), active boutons and passive filopodia ($g_{Na,bouton}$ = 50 mS cm$^{-2}$, $g_{Na,filopodium}$ = 0; intermediate trace), passive boutons and filopodia ($g_{Na,bouton}$ = $g_{Na,filopodium}$ = 0; smallest trace). Note the substantially different $Ca^{2+}$ inflow in the three configurations. Inset schematically depicts the anatomy of MFBs based on serial electron microscopy (from Acsády et al., 1998, with permission from the Society for Neuroscience, Copyright 1998). To facilitate comparison of time courses of $Ca^{2+}$ currents in different conditions, voltage and corresponding $I_{Ca}$ traces in (C) and (D) were shifted in time to align the peaks of the APs. mt, mossy fiber terminal.

synaptic $Na^+$ conductance density in MFBs is comparable to that in nonmyelinated invertebrate axons, as reported previously (120 mS cm$^{-2}$ in squid axons and 40 mS cm$^{-2}$ in Myxicola axons; Hodgkin and Huxley, 1952; Goldman and Schauf, 1973). Furthermore, the presynaptic $Na^+$ channel density in MFBs is in the same range as the density of saxitoxin and tetrodotoxin binding sites in nonmyelinated vertebrate axons (2–200 μm$^{-2}$; Waxman, 1995). Thus, MFBs have highly active properties, comparable to those of peripheral nonmyelinated axons.

In contrast, the $Na^+$ conductance density in MFBs is markedly higher than that in axon initial segments of subicular neurons (Colbert and Johnston, 1996). In this subcellular structure, a current density of 3 pA μm$^{-2}$ was reported, corresponding to a conductance density of ~70 pS μm$^{-2}$ (after correction for open probability and $Na^+$ current reversal potential; Colbert and Johnston, 1996). The $Na^+$ conductance density in MFBs is also substantially higher than that in dendrites of neocortical layer 5 pyramidal neurons (80 pS μm$^{-2}$, after correction for maximum open probability; Stuart and Sakmann, 1994; Häusser et al., 2000), olfactory mitral cells (170 pS μm$^{-2}$; Bischofberger and Jonas, 1997), and hippocampal oriens-alveus interneurons (210 pS μm$^{-2}$; Martina et al., 2000). Thus, the present results suggest that the axon and the presynaptic terminals represent the most excitable subcellular compartments of a neuron. This is consistent with the view that the preferential site of AP initiation is located downstream of the axon initial segment (Colbert and Johnston, 1996).

### Gating Properties and Possible Molecular Identity of the Presynaptic $Na^+$ Channel

Are the gating properties of presynaptic $Na^+$ channels in MFBs specialized to generate rapid and reliable conduction in mossy fiber axons? In comparison to $Na^+$ channels in other cells or subcellular compartments, several similarities are apparent, including fast and highly voltage-dependent activation, high maximum

open probability (0.53 at 0 mV, this paper; 0.59 at –5 mV, Sigworth, 1980), and relatively small single-channel conductance (12 pS calculated from single-channel current, Figure 1C, and reversal potential, Figure 2B, inset; Fenwick et al., 1982; Hille, 2001). Thus, the basic mechanisms of voltage-dependent activation and ion permeation of $Na^+$ channels are conserved.

However, our results suggest that the presynaptic $Na^+$ channels have specialized inactivation properties. We found that the time constant of onset of inactivation of the presynaptic $Na^+$ channels was in the submillisecond range (240 μs at 0 mV), and the time constant of recovery from inactivation was 4.7 ms at –120 mV (Figure 4). In contrast, $Na^+$ channels in somata and dendrites of hippocampal principal neurons show an onset of inactivation that is approximately two times slower, and they have a prominent slow component in the recovery from inactivation (100 ms at –120 mV; Martina and Jonas, 1997; Colbert et al., 1997; Jung et al., 1997; Ellerkmann et al., 2001). As the time course of recovery of $Na^+$ channels from inactivation sets the duration of the refractory period, the fast recovery in MFBs ensures reliable AP propagation in mossy fiber axons during repetitive activity.

What is the molecular identity of the presynaptic $Na^+$ channel in MFBs? In situ hybridization analysis showed that Nav1.2 and Nav1.6 subunit mRNAs are highly expressed in granule cells, whereas other Nav $\alpha$ subunit mRNAs are largely absent (Felts et al., 1997; Schaller and Caldwell, 2000). Furthermore, $\beta$2 and $\beta$3 subunits are abundantly expressed in granule cells, whereas other $\beta$ subunits are barely detectable (Morgan et al., 2000; Yu et al., 2003). Immunocytochemical analysis revealed abundant Nav1.2 immunoreactivity in the mossy fiber tract (Westenbroek et al., 1989; Gong et al., 1999). Nav1.6 immunoreactivity in this region has not been examined yet, but Nav1.2 and Nav1.6 are frequently colocalized in nonmyelinated axons throughout the central nervous system (Caldwell et al., 2000). Thus, it is likely that the presynaptic $Na^+$ channels in MFBs are formed by a mosaic of Nav1.2 $\alpha/\beta$ and Nav1.6 $\alpha/\beta$ heteromers. The fast recovery from inactivation of recombinantly expressed Nav1.2 $\alpha/\beta$ and Nav1.6 $\alpha/\beta$ channels further supports this view (Smith et al., 1998).

### The Presynaptic AP at En Passant versus Terminal Boutons

Can we extrapolate from the active properties of MFBs to other axons and synapses? In the hippocampus, cortex, and cerebellum, the majority of boutons show en passant structure, suggesting that the mechanisms of AP conduction may be similar to those in the mossy fiber pathway. Consistent with this hypothesis, $Ca^{2+}$ transients in en passant boutons of neocortical pyramidal cells are evoked reliably by somatic stimuli (Cox et al., 2000; Koester and Sakmann, 2000). Likewise, in the neurohypophysis, several large hormone-releasing varicosities emerge from parent axons in an en passant manner. As in the MFBs, these varicosities are endowed with voltage-gated $Na^+$ channels (Jackson and Zhang, 1995).

In contrast, the structural and functional mechanisms of AP propagation appear to be very different for the two most extensively studied synapses, the neuromuscular junction (NMJ) and the calyx of Held in the brainstem. In the NMJ, voltage-gated $Na^+$ channels are concentrated at preterminal heminodes adjacent to the synaptic region (Hille, 2001). In the presynaptic terminal, $K^+$ channels predominate, whereas $Na^+$ channels are absent (lizard: Lindgren and Moore, 1989; mouse: Brigant and Mallart, 1982; Dreyer and Penner, 1987). Likewise, in the calyx of Held in the medial nucleus of the trapezoid body (von Gersdorff and Borst, 2002), $Na^+$ channel are clustered near the heminode and are absent from the presynaptic terminal (R.M. Leão et al., 2004, Soc. Neurosci., abstract). Thus in both NMJ and the calyx of Held, invasion of the AP is passive, in contrast to the MFB.

### Functional Significance of Active Boutons: Strength, Reliability, and Timing of Synaptic Transmission

Although voltage-gated $Na^+$ channels are widely associated with action potential initiation and propagation, our computational analysis, based on a reduced axon-multibouton model of morphology and an experimentally constrained model of voltage-gated $Na^+$ channel gating, indicates that the presence of $Na^+$ channels in MFBs has several unexpected consequences for synaptic transmission.

First, the major function of $Na^+$ channels in MFBs appears to be the amplification of AP amplitude at the presynaptic sites. Active boutons boost the presynaptic AP by ~40 mV in comparison to passive boutons. Because of the high activation threshold of presynaptic $Ca^{2+}$ channels (Bischofberger et al., 2002), this amplification translates into an ~2-fold increase in presynaptic $Ca^{2+}$ inflow (Figure 7C). As exocytosis is triggered by cooperative binding of 4–5 $Ca^{2+}$ ions to the $Ca^{2+}$ sensor (Schneggenburger and Neher, 2000), the amount of transmitter release could be increased up to ~$2^4$ (16-fold). $Na^+$ channels in MFBs, together with expression of high-threshold $Ca^{2+}$ channels and the cooperativity of the $Ca^{2+}$ sensor of exocytosis, will boost AP-evoked transmitter release and thus maximize the "signal-to-noise ratio" of synaptic transmission.

Second, $Na^+$ channels in MFBs influence the reliability and velocity of AP propagation (Figure 7A). However, presynaptic $Na^+$ channels are generally less important than axonal $Na^+$ channels.

Third, unexpectedly, $Na^+$ channels in MFBs help to limit the duration of the presynaptic AP (Figure 7B). Intuitively, presynaptic $Na^+$ channels, via a boosting of AP amplitude, enhance the activation of presynaptic $K^+$ channels (Geiger and Jonas, 2000). Both rapid inactivation of presynaptic $Na^+$ channels and fast activation of presynaptic $K^+$ channels will increase the rate of repolarization, contributing to the brief time course of the AP. This situation is different from that at the calyx of Held, where the *absence* of $Na^+$ channels in the presynaptic terminal is required to maintain the brief duration of the presynaptic AP (R.M. Leão et al., 2004, Soc. Neurosci., abstract). Different structural properties (en passant versus terminal bouton) may explain the very different effects of $Na^+$ channels at the two types of synapses.

Fourth, presynaptic $Na^+$ channels appear to be

essential for the efficient charging of filopodial extensions, which form synapses on GABAergic interneurons in the stratum lucidum (Acsády et al., 1998; Lawrence and McBain, 2003). In the case of active filopodia, AP reflections at the sealed end can increase the local AP amplitude beyond that in the main bouton. This may explain the high release probability at filopodial extension-interneuron synapses (Lawrence and McBain, 2003; Lawrence et al., 2004).

### Information Processing in the Mossy Fiber Axon?

High basal synaptic strength and the capability to undergo ~10-fold changes in synaptic strength are hallmarks of the hippocampal mossy fiber synapse (Salin et al., 1996; Henze et al., 2002; Lawrence and McBain, 2003). Although facilitation, posttetanic potentiation, and long-term potentiation are expressed presynaptically at this synapse (Salin et al., 1996), the molecular targets have not been identified. $Na^+$ channels in MFBs will help to establish a high basal synaptic efficacy by boosting the amplitude of the presynaptic AP. Whether presynaptic $Na^+$ channels are also involved in the regulation of synaptic strength is less clear. Nonmyelinated axons hyperpolarize in response to tetanic stimulation, presumably due to the activation of electrogenic $Na^+$/$K^+$ pumps or $Ca^{2+}$-activated $K^+$ channels (Ritchie and Straub, 1957). This could promote recovery of presynaptic $Na^+$ channels from inactivation and thus lead to activity-dependent boosting of the presynaptic AP. In contrast, $Na^+$ channel phosphorylation via PKA or PKC (Carr et al., 2003) or retrieval of presynaptic $Na^+$ channels by endocytosis via $Ca^{2+}$-dependent interactions with synaptotagmin (Sampo et al., 2000) could reduce the number of presynaptic $Na^+$ channels and, thus, may reduce the amplitude of the presynaptic AP.

The contribution of $Na^+$ channels in MFBs to presynaptic AP amplitude, reliability of propagation, and precise spike timing is likely to be critically important for the storage of episodic memory in the hippocampus (Lisman, 1999). It has been proposed that the CA3 region is an autoassociative network, in which the detonator function of the mossy fiber synapse drives the induction of spike timing-dependent plasticity in CA3-CA3 synapses (Lisman, 1999; Kobayashi and Poo, 2004). Furthermore, it has been suggested that the dentate gyrus may be a heteroassociative network. To link two consecutive items by spike timing-dependent plasticity at perforant path-granule cell synapses, the action potentials encoding the two items must be separated in time by the spacing of two $\gamma$ cycles (20 ms; Jensen and Lisman, 1996). This would require a polysynaptic connection among granule cells, e.g., by the pathway granule cell → CA3 pyramidal neuron → mossy cell → granule cell, which plays back the APs in the granule cells encoding a first item to the granule cells encoding the second item in a sequence. For efficient induction of spike timing-dependent plasticity, long delays, but also high reliability and temporal precision of conduction, would be necessary. The mossy fiber axon with the linear array of active boutons appears to be an ideal design to implement such a reliable delay line for heteroassociative memory.

## Experimental Procedures

### Presynaptic Recording

Transverse 250 μm thick slices were cut from the hippocampus of 20 to 24-day-old Wistar rats, primarily with a custom-built vibratome (Geiger et al., 2002). The animals were killed by decapitation, in accordance with national and institutional guidelines. Slices were kept at 35°C for 30 min after slicing and then at room temperature. For the dissection and storage of slices, a solution containing 87 mM NaCl, 25 mM $NaHCO_3$, 10 mM glucose, 75 mM sucrose, 2.5 mM KCl, 1.25 mM $NaH_2PO_4$, 0.5 mM $CaCl_2$, and 7 mM $MgCl_2$ was used. For experiments, the slices were superfused with physiological saline containing 125 mM NaCl, 25 mM $NaHCO_3$, 25 mM glucose, 2.5 mM KCl, 1.25 mM $NaH_2PO_4$, 2 mM $CaCl_2$, and 1 mM $MgCl_2$ (equilibrated with 95% $O_2$/5% $CO_2$ gas mixture).

Patch pipettes were pulled from borosilicate glass tubing (2.0 mm outer diameter, 0.5 mm wall thickness) and filled with a solution containing 145 mM CsCl, 2 mM $MgCl_2$, 2 mM $Na_2ATP$, 0.5 mM $Na_2GTP$, 5 mM $Na_2$-phosphocreatine, 10 mM EGTA, and 10 mM HEPES (pH adjusted to 7.3 with CsOH); pipette resistance was 5–12 MΩ. Mossy fiber boutons in *stratum lucidum* of the hippocampal CA3 region (mainly CA3b) were identified by their small diameter (3–4 μm), the small capacitance (0.8–2 pF whole-cell capacitance readout of the amplifier), and the high input resistance (>1 GΩ; Geiger and Jonas, 2000). All recordings were made from isolated outside-out patches. As outside-out patches were obtained from the center of visualized MFBs and had much smaller surface areas (4 $\mu m^2$, Figures 1E and 1F) than whole boutons (50 $\mu m^2$), it is unlikely that the patches contained a significant amount of axonal membrane. Currents were recorded with an Axopatch 200A amplifier (Axon Instruments, Foster City, CA), filtered at 10 kHz (internal 4-pole low-pass Bessel filter), and sampled at 40 kHz using a CED 1401plus or 1401power interface (Cambridge Electronic Design, Cambridge, UK). Pulse sequences were generated using FPulse (home-made) running under Igor (version 5.01; Lake Oswego, OR) on a personal computer, and filtered with a 2.5 μs RC filter at the amplifier input. To isolate $Na^+$ currents pharmacologically, 20 mM tetraethylammonium chloride (TEA), 3 mM 4-aminopyridine (4-AP), and 100 μM $CdCl_2$ were added to the bath solution. Capacitive and leakage currents were subtracted using the pipette capacitance compensation circuit of the amplifier and a P/–4 method. Patches were held at –80 mV throughout the experiment. For comparison, a subset of recordings was made from outside-out patches isolated from granule cell somata (Figures 3D and 4D). Chemicals were obtained from Sigma, Merck, Riedel-de Haën, or Gerbu. Recordings were made at 23 ± 2°C.

Capacitive transients from outside-out patches (Figures 1E and 1F) were recorded before and after pushing the pipette tip ~10 μm into an insulating ball (1 mm diameter) of Sylgard 184 (Dow Corning, Midland, MI; Sakmann and Neher, 1995). Care was taken to maintain the immersion depth of the pipette. Test pulse amplitude was 50 mV, the filter frequency was 10–50 kHz, and the sampling frequency was 40–100 kHz. Average traces from 100 single sweeps in the two conditions were subtracted, and the area under the transient component was obtained by integration over the initial 100 μs after leakage current subtraction. Capacitance was converted into membrane area assuming a specific membrane capacitance of 1 $\mu F\ cm^{-2}$. Estimates of patch area based on direct capacitance recording under our experimental conditions were approximately two times larger than values obtained in Sakmann and Neher (1995; regression line in their Figure 8).

### Data Analysis

The maximal $Na^+$ conductance ($g_{Na}$ "bar"; Hodgkin and Huxley, 1952; Goldman and Schauf, 1973) was determined as $I_{peak}/[(V - V_{Na}) \times p_{open} \times A]$, where $I_{peak}$ is the peak current, $V_{Na}$ is the $Na^+$ current reversal potential (75.6 mV), $p_{open}$ is the maximum open probability, and A is the estimated patch area. As the membrane broken by the suction pulse resealed frequently, empty patches

were possibly vesicles, and were therefore not considered in the calculation of $g_{Na}$. For kinetic analysis, current traces were left-shifted with respect to the pulse protocol by 32.9 μs to account for the delay introduced by 10 kHz low-pass filtering. The time course of $Na^+$ channel activation was fitted with an exponential function with delayed onset $I(t) = I_0 (1- \exp[-(t - \delta)/\tau_a])$ for $t \geq \delta$ and 0 for $t < 0$, where $I_0$ is the amplitude, $\tau_a$ the activation time constant, and $\delta$ the delay. The time course of deactivation was fitted with either a single exponential or the sum of two exponentials ($V \geq -50$ mV); in the biexponential fit, the fast decay time constant was taken as the deactivation time constant (Oxford, 1981). Activation and inactivation data of each patch were fitted with a Boltzmann function of the form $f(V) = [1 + \exp[(V_{mid}-V)/k]]^{-1}$, where $V_{mid}$ is the midpoint potential and k is the slope factor. Values of $V_{mid}$ and k given in the text are means of results from individual experiments.

For nonstationary fluctuation analysis (Sigworth, 1980), 60–100 $Na^+$ current traces were analyzed. To minimize errors due to rundown, the entire data set was divided into nonoverlapping subsets of ten traces. Mean ensemble current and ensemble variance versus time were determined for each subset and averaged. Variance-mean data were fitted with a parabolic function $\sigma^2(I) = iI - I^2/N + \sigma^2_0$, where $\sigma^2$ is variance, I is the mean current, i is the single-channel current, N is the number of available channels in the patch, and $\sigma^2_0$ is the variance of the baseline noise (Sigworth, 1980). Confidence intervals of i and N were obtained by bootstrap procedures. One hundred artificial data sets were generated by random permutation of elements in adjacent subsets and analyzed as the original data set. Errors were then estimated from percentile intervals (Efron and Tibshirani, 1998).

Curve fitting was performed using Stimfit (home-made) or Mathematica 4.1.2 (Wolfram Research, Champaign, IL). Membrane potentials are given without correction for liquid junction potentials. The values given in the text and the symbols and error bars in the figures indicate mean ± SEM. Differences between presynaptic and somatic patches were tested for statistical significance using a two-sided Student's t test at the significance level (P) indicated.

### Modeling of $Na^+$ Channel Gating and AP Propagation in Axon-Multibouton Structures

As inaccuracies in $Na^+$ channel gating models markedly affect the properties of AP shape and conduction in simulations (Sangrey et al., 2004), a gating model for the MFB $Na^+$ channel was developed. The total data set comprised of activation curve, steady-state inactivation curve, activation time constant, deactivation time constant, onset of inactivation, and recovery from inactivation was fitted with a Hodgkin-Huxley model (HH model) (Hodgkin and Huxley, 1952). For fitting inactivation, steady-state inactivation and time constants were calculated as $h_\infty = \alpha_h/(\alpha_h + \beta_h)$ and $\tau_h = 1/(\alpha_h + \beta_h)$, respectively, and directly compared against the measured values of $h_\infty$ and $\tau_h$. For fitting voltage dependence of activation, steady-state activation and time constants were calculated as $m_\infty = \alpha_m/(\alpha_m + \beta_m)$ and $\tau_m = 1/(\alpha_m + \beta_m)$, and $m_\infty{}^3$ was compared against the measured activation curve. For fitting the time constants of activation, $Na^+$ currents were simulated as $m(t)^3$, with $m(t) = m_\infty - (m_\infty - m_0) \exp(-t/\tau_m)$. Simulated currents were fitted with exponential functions, and activation and deactivation time constants obtained from the fit were compared to the measured data. The sum of squares of differences between experimental observations and model predictions was minimized using FindMinimum of Mathematica. Weight factors were set to the inverse of the maximum value in the data set for kinetic data and to 3 × the inverse of the maximum value for activation and inactivation curves.

Simulations were performed using NEURON 5.6 for Windows (Hines and Carnevale, 1997). The passive electrical properties of the axon-multibouton structure were assumed to be uniform, with a specific membrane capacitance $C_m$ of 1 μF $cm^{-2}$, a specific membrane resistance $R_m$ of 10,000 Ω $cm^2$, and an intracellular resistivity $R_i$ of 110 Ω cm (Hallermann et al., 2003). The structure of the mossy fiber axon-multibouton structure was approximated by a soma (diameter, 10 μm), 10 axonal cylinders (diameter, 0.2 μm; length, 100 μm), and ten en passant boutons (diameter, 4 μm) placed between adjacent axonal segments. Thus, axonal segments and boutons had comparable surface areas (63 $\mu m^2$ for each axonal segment, 50 $\mu m^2$ for each bouton). In a subset of simulations (Figure 7E), filopodial extensions with a small terminal bouton (filopodium diameter, 0.1 μm, and length, 30 μm; bouton diameter, 1 μm; Acsády et al., 1998) were added to each large bouton. For axons and filopodia, the number of segments was 1 $\mu m^{-1}$. For soma and boutons, the number of segments was 1 and 10, respectively. The time step was 5 μs in all simulations. The resting potential was assumed as –80 mV, consistent with the values of resting potentials in MFB recordings in which seal resistance >> input resistance (Geiger and Jonas, 2000). The reversal potential of the leak conductance was set to –81 mV to maintain stability. Voltage-gated $Na^+$ channels, $K^+$ channels, and leak channels were inserted into soma, axon, and boutons as indicated. The somatic $Na^+$ conductance density was set to 10 mS $cm^{-2}$ (20% of the standard axoboutonal conductance density) throughout. APs were evoked by injection of depolarizing current into the soma (2 ms, 0.2 nA). $Na^+$ channels were implemented as the HH model obtained by fitting our experimental data (Figure 5). The voltage dependence of both activation and inactivation was shifted by 12 mV toward positive potentials to account for differences in the Donnan potential between whole-cell and isolated patch configuration (Fenwick et al., 1982; Marty and Neher, 1995).

$K^+$ channels were implemented as a HH $K^+$ channel model, with $\alpha(V) = 0.01\ ms^{-1} - (V + 55\ mV)/(\exp[- (V + 55\ mV)/10\ mV] - 1)$ and $\beta(V) = 0.125\ ms^{-1} \exp[- (V + 65\ mV)/80\ mV]$ (Hodgkin and Huxley, 1952), which provides a relatively accurate description of the voltage-dependence of activation of $K^+$ channels in MFBs (at 34°C; Geiger and Jonas, 2000). The $K^+$ channel conductance density was set to 36 mS $cm^{-2}$ throughout. In the experiments in which trains of high-frequency stimuli were applied (Figures 6C and 6D), $K^+$ channel inactivation was implemented multiplicatively; the gating parameters were based on published inactivation properties of recombinant Kv1.4 channels with $\alpha(V) = 0.0000256077\ ms^{-1} \exp[-V/45.4217\ mV]$ and $\beta(V) = 0.0330402\ ms^{-1} (\exp[-(V + 45.6599\ mV)/2.30235\ mV] + 1)$ (Wissmann et al., 2003). The equilibrium potentials for $Na^+$ and $K^+$ ions were assumed as +50 mV and –85 mV, respectively.

### Acknowledgments

We thank Drs. J. Bischofberger and M. Heckmann for critically reading the manuscript, K. Winterhalter and M. Northemann for technical assistance, and U. Fröbe for programming. We are also grateful to H. von Gersdorff for sharing unpublished results. Supported by the Deutsche Forschungsgemeinschaft (SFB505/C5).

Received: November 12, 2004
Revised: December 23, 2004
Accepted: December 28, 2004
Published: February 2, 2005

### References

Acsády, L., Kamondi, A., Sík, A., Freund, T., and Buzsáki, G. (1998). GABAergic cells are the major postsynaptic targets of mossy fibers in the rat hippocampus. J. Neurosci. *18*, 3386–3403.

Amaral, D.G., Ishizuka, N., and Claiborne, B. (1990). Neurons, numbers and the hippocampal network. Prog. Brain Res. *83*, 1–11.

Bezanilla, F., and Armstrong, C.M. (1977). Inactivation of the sodium channel. I. Sodium current experiments. J. Gen. Physiol. *70*, 549–566.

Bischofberger, J., and Jonas, P. (1997). Action potential propagation into the presynaptic dendrites of rat mitral cells. J. Physiol. *504*, 359–365.

Bischofberger, J., and Jonas, P. (2002). TwoB or not twoB: differential transmission at glutamatergic mossy fiber-interneuron synapses in the hippocampus. Trends Neurosci. *25*, 600–603.

Bischofberger, J., Geiger, J.R.P., and Jonas, P. (2002). Timing and

efficacy of $Ca^{2+}$ channel activation in hippocampal mossy fiber boutons. J. Neurosci. *22*, 10593–10602.

Brigant, J.L., and Mallart, A. (1982). Presynaptic currents in mouse motor endings. J. Physiol. *333*, 619–636.

Caldwell, J.H., Schaller, K.L., Lasher, R.S., Peles, E., and Levinson, S.R. (2000). Sodium channel $Na_v1.6$ is localized at nodes of Ranvier, dendrites, and synapses. Proc. Natl. Acad. Sci. USA *97*, 5616–5620.

Carr, D.B., Day, M., Cantrell, A.R., Held, J., Scheuer, T., Catterall, W.A., and Surmeier, D.J. (2003). Transmitter modulation of slow, activity-dependent alterations in sodium channel availability endows neurons with a novel form of cellular plasticity. Neuron *39*, 793–806.

Chicurel, M.E., and Harris, K.M. (1992). Three-dimensional analysis of the structure and composition of CA3 branched dendritic spines and their synaptic relationships with mossy fiber boutons in the rat hippocampus. J. Comp. Neurol. *325*, 169–182.

Colbert, C.M., and Johnston, D. (1996). Axonal action-potential initiation and $Na^+$ channel densities in the soma and axon initial segment of subicular pyramidal neurons. J. Neurosci. *16*, 6676–6686.

Colbert, C.M., Magee, J.C., Hoffman, D.A., and Johnston, D. (1997). Slow recovery from inactivation of $Na^+$ channels underlies the activity-dependent attenuation of dendritic action potentials in hippocampal CA1 pyramidal neurons. J. Neurosci. *17*, 6512–6521.

Cox, C.L., Denk, W., Tank, D.W., and Svoboda, K. (2000). Action potentials reliably invade axonal arbors of rat neocortical neurons. Proc. Natl. Acad. Sci. USA *97*, 9724–9728.

Debanne, D. (2004). Information processing in the axon. Nat. Rev. Neurosci. *5*, 304–316.

Debanne, D., Guérineau, N.C., Gähwiler, B.H., and Thompson, S.M. (1997). Action-potential propagation gated by an axonal $I_A$-like $K^+$ conductance in hippocampus. Nature *389*, 286–289.

Dreyer, F., and Penner, R. (1987). The actions of presynaptic snake toxins on membrane currents of mouse motor nerve terminals. J. Physiol. *386*, 455–463.

Efron, B., and Tibshirani, R.J. (1998). An Introduction to the Bootstrap (London: Chapman & Hall/CRC).

Ellerkmann, R.K., Riazanski, V., Elger, C.E., Urban, B.W., and Beck, H. (2001). Slow recovery from inactivation regulates the availability of voltage-dependent $Na^+$ channels in hippocampal granule cells, hilar neurons and basket cells.. J. Physiol. *532*, 385–397. Erratum: J. Physiol. *533*, 921, 2001.

Felts, P.A., Yokoyama, S., Dib-Hajj, S., Black, J.A., and Waxman, S.G. (1997). Sodium channel $\alpha$-subunit mRNAs I, II, III, NaG, Na6 and hNE (PN1): different expression patterns in developing rat nervous system. Brain Res. Mol. Brain Res. *45*, 71–82.

Fenwick, E.M., Marty, A., and Neher, E. (1982). Sodium and calcium channels in bovine chromaffin cells. J. Physiol. *331*, 599–635.

Geiger, J.R.P., and Jonas, P. (2000). Dynamic control of presynaptic $Ca^{2+}$ inflow by fast-inactivating $K^+$ channels in hippocampal mossy fiber boutons. Neuron *28*, 927–939.

Geiger, J.R.P., Bischofberger, J., Vida, I., Fröbe, U., Pfitzinger, S., Weber, H.J., Haverkampf, K., and Jonas, P. (2002). Patch-clamp recording in brain slices with improved slicer technology. Pflügers Arch. *443*, 491–501.

Goldman, L., and Schauf, G.L. (1973). Quantitative description of sodium and potassium currents and computed action potentials in *Myxicola* giant axons. J. Gen. Physiol. *61*, 361–384.

Goldstein, S.S., and Rall, W. (1974). Changes of action potential shape and velocity for changing core conductor geometry. Biophys. J. *14*, 731–757.

Gong, B., Rhodes, K.J., Bekele-Arcuri, Z., and Trimmer, J.S. (1999). Type I and type II $Na^+$ channel $\alpha$-subunit polypeptides exhibit distinct spatial and temporal patterning, and association with auxiliary subunits in rat brain. J. Comp. Neurol. *412*, 342–352.

Häusser, M., Spruston, N., and Stuart, G.J. (2000). Diversity and dynamics of dendritic signaling. Science *290*, 739–744.

Hallermann, S., Pawlu, C., Jonas, P., and Heckmann, M. (2003). A large pool of releasable vesicles in a cortical glutamatergic synapse. Proc. Natl. Acad. Sci. USA *100*, 8975–8980.

Henze, D.A., Wittner, L., and Buzsáki, G. (2002). Single granule cells reliably discharge targets in the hippocampal CA3 network *in vivo*. Nat. Neurosci. *5*, 790–795.

Hille, B. (2001). Ion Channels of Excitable Membranes (Sunderland, MA: Sinauer).

Hines, M.L., and Carnevale, N.T. (1997). The NEURON simulation environment. Neural Comput. *9*, 1179–1209.

Hodgkin, A.L., and Huxley, A.F. (1952). A quantitative description of membrane current and its application to conduction and excitation in nerve. J. Physiol. *117*, 500–544.

Jackson, M.B., and Zhang, S.J. (1995). Action potential propagation and propagation block by GABA in rat posterior pituitary nerve terminals. J. Physiol. *483*, 597–611.

Jensen, O., and Lisman, J.E. (1996). Hippocampal CA3 region predicts memory sequences: accounting for the phase precession of place cells. Learn. Mem. *3*, 279–287.

Jung, H.Y., Mickus, T., and Spruston, N. (1997). Prolonged sodium channel inactivation contributes to dendritic action potential attenuation in hippocampal pyramidal neurons. J. Neurosci. *17*, 6639–6646.

Katz, B. (1969). The Release of Neural Transmitter Substances (Liverpool: Liverpool University Press).

Katz, B., and Miledi, R. (1965). Propagation of electric activity in motor nerve terminals. Proc. R. Soc. Lond. B. Biol. Sci. *161*, 453–482.

Kobayashi, K., and Poo, M.M. (2004). Spike train timing-dependent associative modification of hippocampal CA3 recurrent synapses by mossy fibers. Neuron *41*, 445–454.

Koester, H.J., and Sakmann, B. (2000). Calcium dynamics associated with action potentials in single nerve terminals of pyramidal cells in layer 2/3 of the young rat neocortex. J. Physiol. *529*, 625–646.

Lawrence, J.J., and McBain, C.J. (2003). Interneuron diversity series: containing the detonation—feedforward inhibition in the CA3 hippocampus. Trends Neurosci. *26*, 631–640.

Lawrence, J.J., Grinspan, Z.M., and McBain, C.J. (2004). Quantal transmission at mossy fibre targets in the CA3 region of the rat hippocampus. J. Physiol. *554*, 175–193.

Lindgren, C.A., and Moore, J.W. (1989). Identification of ionic currents at presynaptic nerve endings of the lizard. J. Physiol. *414*, 201–222.

Lisman, J.E. (1999). Relating hippocampal circuitry to function: recall of memory sequences by reciprocal dentate-CA3 interactions. Neuron *22*, 233–242.

Lüscher, H.R., and Shiner, J.S. (1990a). Computation of action potential propagation and presynaptic bouton activation in terminal arborizations of different geometries. Biophys. J. *58*, 1377–1388.

Lüscher, H.R., and Shiner, J.S. (1990b). Simulation of action potential propagation in complex terminal arborizations. Biophys. J. *58*, 1389–1399.

Manor, Y., Koch, C., and Segev, I. (1991). Effect of geometrical irregularities on propagation delay in axonal trees. Biophys. J. *60*, 1424–1437.

Martina, M., and Jonas, P. (1997). Functional differences in $Na^+$ channel gating between fast-spiking interneurones and principal neurones in rat hippocampus. J. Physiol. *505*, 593–603.

Martina, M., Vida, I., and Jonas, P. (2000). Distal initiation and active propagation of action potentials in interneuron dendrites. Science *287*, 295–300.

Marty, A., and Neher, E. (1995). Tight-seal whole-cell recording. In Single-Channel Recording, B. Sakmann and E. Neher, eds. (New York: Plenum), pp. 31–52.

Morgan, K., Stevens, E.B., Shah, B., Cox, P.J., Dixon, A.K., Lee, K., Pinnock, R.D., Hughes, J., Richardson, P.J., Mizuguchi, K., and Jackson, A.P. (2000). $\beta$3: an additional auxiliary subunit of the voltage-sensitive sodium channel that modulates channel gating with distinct kinetics. Proc. Natl. Acad. Sci. USA *97*, 2308–2313.

Oxford, G.S. (1981). Some kinetic and steady-state properties of

sodium channels after removal of inactivation. J. Gen. Physiol. *77*, 1–22.

Ritchie, J.M., and Straub, R.W. (1957). The hyperpolarization which follows activity in mammalian non-medullated fibres. J. Physiol. *136*, 80–97.

Ruiz, A., Fabian-Fine, R., Scott, R., Walker, M.C., Rusakov, D.A., and Kullmann, D.M. (2003). $GABA_A$ receptors at hippocampal mossy fibers. Neuron *39*, 961–973.

Sabatini, B.L., and Regehr, W.G. (1999). Timing of synaptic transmission. Annu. Rev. Physiol. *61*, 521–542.

Sakmann, B., and Neher, E. (1995). Geometric parameters of pipettes and membrane patches. In Single-Channel Recording, B. Sakmann and E. Neher, eds. (New York: Plenum), pp. 637–650.

Salin, P.A., Scanziani, M., Malenka, R.C., and Nicoll, R.A. (1996). Distinct short-term plasticity at two excitatory synapses in the hippocampus. Proc. Natl. Acad. Sci. USA *93*, 13304–13309.

Sampo, B., Tricaud, N., Leveque, C., Seagar, M., Couraud, F., and Dargent, B. (2000). Direct interaction between synaptotagmin and the intracellular loop I–II of neuronal voltage-sensitive sodium channels. Proc. Natl. Acad. Sci. USA *97*, 3666–3671.

Sangrey, T.D., Friesen, W.O., and Levy, W.B. (2004). Analysis of the optimal channel density of the squid giant axon using a reparameterized Hodgkin-Huxley model. J. Neurophysiol. *91*, 2541–2550.

Schaller, K.L., and Caldwell, J.H. (2000). Developmental and regional expression of sodium channel isoform NaCh6 in the rat central nervous system. J. Comp. Neurol. *420*, 84–97.

Schmitz, D., Frerking, M., and Nicoll, R.A. (2000). Synaptic activation of presynaptic kainate receptors on hippocampal mossy fiber synapses. Neuron *27*, 327–338.

Schneggenburger, R., and Neher, E. (2000). Intracellular calcium dependence of transmitter release rates at a fast central synapse. Nature *406*, 889–893.

Sigworth, F.J. (1980). The variance of sodium current fluctuations at the node of Ranvier. J. Physiol. *307*, 97–129.

Smith, M.R., Smith, R.D., Plummer, N.W., Meisler, M.H., and Goldin, A.L. (1998). Functional analysis of the mouse Scn8a sodium channel. J. Neurosci. *18*, 6093–6102.

Stuart, G.J., and Sakmann, B. (1994). Active propagation of somatic action potentials into neocortical pyramidal cell dendrites. Nature *367*, 69–72.

Taddese, A., and Bean, B.P. (2002). Subthreshold sodium current from rapidly inactivating sodium channels drives spontaneous firing of tuberomammillary neurons. Neuron *33*, 587–600.

von Gersdorff, H., and Borst, J.G.G. (2002). Short-term plasticity at the calyx of Held. Nat. Rev. Neurosci. *3*, 53–64.

Waxman, S.G. (1995). Voltage-gated ion channels in axons: localization, function, and development. In The Axon, S.G. Waxman, J.D. Kocsis, and P.K. Stys, eds. (New York: Oxford University Press), pp. 218–243.

Westenbroek, R.E., Merrick, D.K., and Catterall, W.A. (1989). Differential subcellular localization of the $R_I$ and $R_{II}$ $Na^+$ channel subtypes in central neurons. Neuron *3*, 695–704.

Wissmann, R., Bildl, W., Oliver, D., Beyermann, M., Kalbitzer, H.-R., Bentrop, D., and Fakler, B. (2003). Solution structure and function of the "tandem inactivation domain" of the neuronal A-type potassium channel Kv1.4. J. Biol. Chem. *278*, 16142–16150.

Yu, F.H., Westenbroek, R.E., Silos-Santiago, I., McCormick, K.A., Lawson, D., Ge, P., Ferriera, H., Lilly, J., DiStefano, P.S., Catterall, W.A., et al. (2003). Sodium channel $\beta 4$, a new disulfide-linked auxiliary subunit with similarity to $\beta 2$. J. Neurosci. *23*, 7577–7585.